



PROF. MEI ZHANG (Orcid ID : 0000-0001-9803-0205)

PROF. BLAKE MEYERS (Orcid ID : 0000-0003-3436-6097)

PROF. NATHAN SPRINGER (Orcid ID : 0000-0002-7301-4759)

Article type : MS - Regular Manuscript

CHH DNA methylation increases at 24-*PHAS* loci depend on 24-nt phasiRNAs in maize meiotic anthers

Mei Zhang^{1,†}, Xuxu Ma^{1,†}, Chunyu Wang^{1,2}, Qing Li³, Blake C. Meyers^{4,5}, Nathan M. Springer³, Virginia Walbot^{6,†}

¹ Key Laboratory of Plant Molecular Physiology, -Institute of Botany, Chinese Academy of Sciences, Nanxincun 20, Fragrant Hill, Beijing 100093, China.

² University of Chinese Academy of Sciences, Beijing 100049, China.

³ Department of Plant and Microbial Biology, University of Minnesota, St. Paul, MN 55108, USA.

⁴ Donald Danforth Plant Science Center, St Louis, MO 63132, USA.

⁵ University of Missouri-Columbia, Division of Plant Sciences, 52 Agriculture Lab, Columbia, MO 65211, USA.

This article has been accepted for publication and undergone full peer review but has not been through the copyediting, typesetting, pagination and proofreading process, which may lead to differences between this version and the [Version of Record](#). Please cite this article as [doi: 10.1111/nph.17060](https://doi.org/10.1111/nph.17060)

This article is protected by copyright. All rights reserved

⁶ Department of Biology, Stanford University, Stanford, CA 94305 USA.

†These authors contributed equally to this work.

Author for correspondence:

Mei Zhang

Tel: +86(10) 6283-6251

Email: mei.zhang@ibcas.ac.cn

Received: 7 July 2020

Accepted: 14 October 2020

ORCID

Mei Zhang <http://orcid.org/0000-0001-9803-0205>
Xuxu Ma <https://orcid.org/0000-0002-3206-8187>
Chunyu Wang <https://orcid.org/0000-0001-7104-3874>
Blake C. Meyers <http://orcid.org/0000-0003-3436-6097>
Nathan M. Springer <http://orcid.org/0000-0002-7301-4759>

1 **Summary**

- 2 ● Plant phasiRNAs contribute to robust male fertility, however, specific functions
3 remain undefined. In maize (*Zea mays*), *male sterile23* (*ms23*), necessary for both
4 24-nt phasiRNA precursor (*24-PHAS*) loci and *Dicer-like5* (*Dcl5*) expression, and
5 *dcl5-1* mutants unable to slice *PHAS* transcripts, lack nearly all 24-nt phasiRNAs.
- 6 ● Based on sequence capture bisulfite-sequencing, we find that CHH DNA methylation
7 of most *24-PHAS* loci is increased in meiotic anthers of control plants but not in the
8 *ms23* and *dcl5* mutants.
- 9 ● Because *dcl5-1* anthers express *PHAS* precursors, we conclude that the 24-nt
10 phasiRNAs, rather than just activation of *PHAS* transcription, are required for
11 targeting increased CHH methylation at these loci.
- 12 ● Although *PHAS* precursors are processed into multiple 24-nt phasiRNA products,
13 there is substantial differential product accumulation. Abundant 24-nt phasiRNA
14 positions corresponded to high CHH methylation within individual loci, reinforcing
15 the conclusion that 24-nt phasiRNAs contribute to increased CHH methylation in *cis*.

16
17

18 **Key words:** phasiRNA, DNA methylation, *Dcl5*, *Ms23*, *Zea mays* (maize)

20 Introduction

21 In flowering plants, small RNAs (sRNAs) are key regulators during reproduction in both
22 the sporophyte and gametophyte (Borges & Martienssen, 2015). Reproductive phasiRNAs
23 were first described in male reproductive organs of maize and rice (Johnson *et al.*, 2009;
24 Song *et al.*, 2012a; Zhai *et al.*, 2015; Fei *et al.*, 2016) and are now known in diverse
25 monocots and eudicots (Kakrana *et al.*, 2018; Xia *et al.*, 2019). Reproductive phasiRNAs
26 exist in two size classes with discrete spatiotemporal regulation in anthers: the “premeiotic”
27 21-nt phasiRNAs are preferentially expressed during the cell fate specification and
28 proliferation period, while the “meiotic” 24-nt phasiRNAs begin to be synthesized at the
29 onset of meiosis and accumulate to high levels during meiosis I (Zhai *et al.*, 2015). The
30 24-nt reproductive phasiRNAs are broadly present in angiosperms, and they may have
31 originated with the evolutionary emergence of anthers (Xia *et al.*, 2015; Shuai *et al.*, 2016;
32 Kakrana *et al.*, 2018; Liu *et al.*, 2018; Yu *et al.*, 2018; Xia *et al.*, 2019).

33 The exact functions of phasiRNAs in anthers are unknown, but they play critical roles
34 in male reproduction. For example, a mutation in long non-coding RNA *PMSIT*, a *PHAS*
35 precursor yielding 21-nt phasiRNAs, is responsible for the agronomically important,
36 photoperiod-sensitive male sterility used in hybrid rice production (Fan *et al.*, 2016). In
37 maize, *dcl5-1* mutants, which are deficient in 24-nt phasiRNAs, exhibit conditional male
38 fertility, with the main defect in tapetal cell differentiation during meiosis (Teng *et al.*,
39 2020). Quantification of *PHAS* precursor transcripts and phasiRNA abundance in several
40 maize male sterile mutants, demonstrated that production of 21-nt phasiRNAs requires
41 normal epidermal development, while 24-nt phasiRNAs require normally developed
42 tapetal cells (Zhai *et al.*, 2015). In rice, tapetal cell differentiation during meiosis is also
43 required for 24-nt phasiRNA biogenesis (Ono *et al.*, 2018). A fascinating aspect of male
44 reproductive phasiRNAs is the parallel with mammalian PIWI-associated RNAs (piRNAs).
45 Like phasiRNAs, there are two size classes, the shorter class accumulating prior to meiosis
46 and the longer class occurring during meiosis (Girard *et al.*, 2006; Grivna *et al.*, 2006;
47 Vagin *et al.*, 2006; Fu & Wang, 2014). Furthermore, like phasiRNAs, piRNAs are
48 required for spermatogenesis (Fu & Wang, 2014), and are partly generated in a phased

49 pattern (Han *et al.*, 2015; Mohn *et al.*, 2015).

50 The current understanding of phasiRNA biogenesis is that the precursors are long,
51 non-coding RNAs transcribed by DNA-DEPENDENT RNA POLYMERASE II (Pol II)
52 from several hundred *PHAS* loci. The production of 21- and 24-nt phasiRNAs is initiated
53 by 22-nt miR2118 or miR2275, directing the cleavage of 21- or 24-*PHAS* primary
54 transcripts, respectively (Johnson *et al.*, 2009; Arikiti *et al.*, 2013; Zhai *et al.*, 2015).
55 RNA-DEPENDENT RNA POLYMERASE 6 (RDR6) converts the resulting 3' cleaved
56 RNA fragments into double-stranded RNA (Song *et al.*, 2012b). This dsRNA is the
57 substrate for phased cleavage by a Dicer enzyme; DCL4 is proposed for 21-nt phasiRNAs
58 and DCL5 for the 24-nt class based on expression timing (Song *et al.*, 2012a; Arikiti *et al.*,
59 2013). *Dcl5* is a duplication of *Dcl3* found in many monocots (Xia *et al.*, 2019). Proof that
60 DCL5 is required for 24-nt phasiRNA biogenesis, but not generation of other small RNAs,
61 comes from analysis of multiple *dcl5* alleles in maize, which lack nearly all 24-nt
62 phasiRNAs (Teng *et al.*, 2020). The entire 24-nt phasiRNA biogenesis pathway appears to
63 be regulated by MS23, a basic helix-loop-helix (bHLH) transcription factor that controls
64 the initial steps in tapetal differentiation. In maize *ms23* mutants with defective tapetum
65 development, *PHAS* precursors, the normal suite of miR2275 types, *Dcl5*, and 24-nt
66 phasiRNAs are missing (Zhai *et al.*, 2015; Nan *et al.*, 2017); additionally, several
67 thousand protein-coding genes are mis-regulated (Nan *et al.*, 2017).

68 Biogenesis of phasiRNAs in grasses parallels that of trans-acting small interfering
69 RNAs (tasiRNAs) (Arikiti *et al.*, 2013; Deng *et al.*, 2018). The tasiRNAs interact with
70 mRNAs and result in mRNA degradation or block translation by virtue of
71 complementarity. *Arabidopsis thaliana* has four *TAS* gene families -- *TAS1*, *TAS2*, *TAS3*,
72 and *TAS4* -- and they are present at eight genetic loci (Allen *et al.*, 2005; Rajagopalan *et*
73 *al.*, 2006). In addition to targeting mRNAs, 21-nt tasiRNAs from *TAS3c* and *TAS1a* were
74 reported to direct DNA methylation at their cognate *TAS*-encoding loci (Wu *et al.*, 2012;
75 Wu, 2013), a type of regulation defined as “in *cis*” in the plant small RNA community.
76 Elevated DNA methylation of the *TAS3c* locus requires DCL1, while multiple DCLs
77 contribute to DNA methylation of *TAS1* loci (Wu *et al.*, 2012; Wu, 2013). Although 24-nt

78 maize phasiRNAs are proposed to be synthesized in the tapetum (Teng *et al.*, 2020), they
79 also accumulate in meiocytes (Zhai *et al.*, 2015). Dukowic-Schulze *et al.* (2016) proposed
80 that phasiRNA could be involved in *cis* DNA methylation at their own loci, because they
81 detected elevated CHH DNA methylation at *PHAS* loci in zygotene stage maize meiocytes
82 and in whole anthers compared to levels in seedlings. In mammalian testes, a small
83 fraction of piRNAs maintain genome integrity by epigenetically silencing transposons via
84 DNA methylation, especially in germline stem cells (Aravin *et al.*, 2007; Le Thomas *et al.*,
85 2013; Luteijn & Ketting, 2013; Fu & Wang, 2014; Zhai *et al.*, 2015); this possible
86 function has not been explored for 24-nt plant phasiRNAs, however, the plant phasiRNAs
87 are not complementary to known transposons.

88 Building on the foundation established by Dukowic-Schulze *et al.* (2016), we wished to
89 address two questions. First, do the 24-*PHAS* loci of anthers acquire elevated CHH DNA
90 methylation after synthesis of the 24-nt phasiRNAs or do anthers have a constitutively
91 elevated level? Second, if there is developmental regulation of CHH DNA methylation,
92 does it occur after transcriptional activation of 24-*PHAS* loci or does it require successful
93 generation of the 24-nt phasiRNA products? To answer these questions and explore the
94 potential role of 24-nt phasiRNAs in maize DNA methylation, we generated sequence
95 capture bisulfite-sequencing data from two male sterile mutants, *dcl5-1* and *ms23*, where
96 24-nt phasiRNAs are highly reduced or eliminated, and their control plants.

97 **MATERIALS AND METHODS**

98 **Plant materials**

99 Maize was grown in a greenhouse at Stanford, CA with a 14-h day (28 °C)/ 10-h night
100 (22 °C) light cycle. Dissected anthers were staged using a micrometer.

101 For the *dcl5* mutant, we utilized the *dcl5-1* allele with a one-base pair deletion in the
102 coding region of the *Dcl5* gene (Teng *et al.*, 2020). We started with the T₀ generation
103 heterozygous *dcl5-1/+* plants in the HiII background. After several generations of
104 self-crossing or crossing among sibling plants, we obtained T₃ and T₄ generation 1:2:1
105 populations for dissecting the anthers of the homozygous *dcl5-1* (*dcl5-1/dcl5-1*) mutant
106 and its wildtype fertile control (+/+). For *ms23*, a 1:2:1 population of *ms23-ref* in the
107 ND101 background introgressed several times into the W23 inbred line was used; anthers
108 from the homozygous *ms23* (*ms23/ms23*) mutant and its fertile control (*ms23/+* or +/+) were
109 collected. To simplify figure labeling, the fully fertile sibling plants compared to
110 mutants in the same family are referred to as “control plants”. Table **S1** provides detailed
111 information about the biological samples.

112 **WGBS library preparation and data analysis**

113 Whole genome bisulfite sequencing (WGBS) was performed using 0.5 mm, 2.0 mm, and
114 4.0 mm W23 anthers. DNA was extracted from each sample using CTAB, and libraries
115 were prepared for WGBS as previously described (Urich *et al.*, 2015). Sequencing was
116 performed on a HiSeq 2000 platform and generated 101-bp paired reads, followed by
117 quality control using FASTQC and adaptor trimming using Trim Galore. For each sample,
118 reads were aligned to the maize B73 reference genome B73_AGPv4 (Jiao *et al.*, 2017) by
119 BSMAP (Xi & Li, 2009). We calculated the methylation level for each cytosine using
120 methratio.py in BSMAP in the uniquely mapped, duplication-removed and properly paired
121 reads.

122 ViewBS was utilized to construct the plots based on WGBS data (Huang *et al.*, 2018).
123 Briefly, the 2 kb up- and down-stream regions of 21- and 24-*PHAS* loci, protein-coding
124 genes, and transposons (TEs), and their body regions were divided into 100, 60, and 100

125 bins, separately. Then, the methylation level of each bin was summarized by dividing
126 detected methylated cytosines (#C) by total cytosines (#C and # delta T) (Schultz *et al.*,
127 2012).

128 **Sequence capture bisulfite-sequencing library preparation and data mapping**

129 To gain high-resolution methylation profiles for 24-*PHAS* loci, we chose ~20,000 specific
130 regions from the B73 genome, including 176 24-*PHAS* and 463 21-*PHAS* loci (Zhai *et al.*,
131 2015). We found that 122 of the 176 24-*PHAS* loci and 416 of 463 21-*PHAS* loci
132 identified in the B73 reference genome v4, contained a predicted miR2275 or miR2118
133 cleavage site (CS), and were used as analyzable *PHAS* loci in our study. The capture
134 probes of those regions were designed by Roche (Han *et al.*, 2018). Briefly, we
135 constructed a standard genome bisulfite library and extracted capture target regions by
136 hybridization to probes as described previously (Li *et al.*, 2014). Then the capture library
137 was sequenced on an Illumina MiSeq instrument using 150 cycles from both ends after
138 PCR amplification. The computational methods described for WGBS data were used to
139 analyze sequence capture bisulfite-sequencing data.

140 To plot the methylation profiles at 21- and 24-*PHAS* loci based on sequence capture
141 bisulfite-sequencing, the 200 bp upstream region, transcribed regions prior to the CS, the
142 transcribed region after the CS, and the 200 bp downstream region were divided into 5, 15,
143 45, and 5 bins, respectively. The same strategy was utilized to calculate the DNA
144 methylation of each bin as for WGBS data.

145 Handling replicate samples: 1) The replicates of 2.0 mm anther of *dcl5-1* mutant and its
146 controls were from the T₃ and T₄ generations; data were analyzed separately for
147 methylation level change among 21-*PHAS* and 24-*PHAS* loci. Subsequently, only the T₃
148 generation data were used, because of the relatively low coverage in the T₄ generation
149 dataset. 2) Regarding the replicates of 1.0 mm anthers, we used the average for the
150 analysis of methylation levels at 24-*PHAS* loci and 21-*PHAS* loci in the *dcl5-1* mutant and
151 its controls in pre-meiotic (0.5 and 1.0 mm) and meiotic 2.0 mm anthers. Other biological
152 samples did not have replicates.

153 **sRNA-seq and RNA-seq library construction and sequencing**

154 sRNA-seq and RNA-seq libraries were prepared as previously described (Mathioni *et al.*,
155 2017; Teng *et al.*, 2020). In brief, total RNA was isolated and libraries were constructed
156 for *dcl5-1* and its wild-type control, with two biological replicates, and sequenced using
157 the Illumina HiSeq2500 platform.

158 For sRNA-seq data, adapters were trimmed by Trim Galore (version 0.6.0), and Bowtie
159 (version 1.2.2) (Langmead *et al.*, 2009) was performed for the alignment with the
160 parameter “-q -e 1 -l 31 -n 0 -p 5 -m 20 -a -S --nomaqround --chunkmbs 524” to the maize
161 B73 reference genome v4. Only uniquely mapped reads were used in this study. The
162 abundance of sRNA is normalized on the basis of the total count of mapped reads in that
163 sample. The abundance of 24-nt phasiRNAs in the *ms23* mutant and its control was
164 calculated based on the published sRNA-seq data from Zhai *et al.* (2015).

165 For RNA-seq data, read quality was checked using Fastp (Chen *et al.*, 2018) and then
166 mapped to the maize B73 reference genome B73_AGpv4 (Jiao *et al.*, 2017) by Hisat2
167 (Kim *et al.*, 2015). Only uniquely aligned reads, as input for StringTie (Pertea *et al.*, 2015),
168 were used to calculate 24-*PHAS* transcript expression levels.

169 **Updating the list of 24-*PHAS* loci in maize anthers**

170 sRNA-seq data from 2.0 mm anthers of the control of the *dcl5-1* mutant were used for
171 24-*PHAS* detection. Only 24-nt intervals were used for genome-wide phasing analysis,
172 and the phasing scores were calculated as previously described (De Paoli *et al.*, 2009).
173 With the criterion of a phasing score higher than 25 plus a manual check, we had an
174 updated list of 151 24-*PHAS* loci, 23 of which were newly identified.

175 **Identification of 24-*PHAS* in the 2.0 mm *dcl5-1* mutant anthers**

176 Considering the relatively low abundance of 24-nt small RNAs mapped to 24-*PHAS* in
177 *dcl5-1* 2.0 mm anthers, we required the largest phasing score of one 24-nt siRNA per
178 locus to be greater than or about 20. For some examples with an obviously good phasing

179 pattern -- at least 3 continuous and high phasing score elements with a 24-nt spacing
180 interval by manual checking -- the largest phasing score can be low as 15.

181 **CHH DMR detection**

182 To detect differentially methylated regions, we summarized CHH methylation levels for
183 each 50-bp non-overlapping sliding window with CHHs and at least 10 reads, dividing
184 detected methylated cytosines (#C) by total cytosines (#C and # delta T). Then, the
185 *p*-value of Fisher's exact test was calculated for each window, to weigh the significance of
186 allele bias. The criteria were as follows: 1) Q-values (converted by *p*-value) < 0.05
187 between the DNA methylation level of the mutant and its control; 2) absolute methylation
188 difference between wild-type and mutant > 5%; 3) and the change relative to wild-type
189 $((\text{wild-type} - \text{mutant})/\text{wild-type})$ greater than 40%. Finally, we combined the adjoining
190 windows detected as DMRs within 200 bp, and then recalculated the percentage using the
191 same strategy.

192 **Abundant 24-nt siRNA position detection**

193 Because we observed that 24-nt phasiRNAs are unevenly distributed across individual
194 24-*PHAS* loci, we defined the 24-nt siRNA with the highest number of normalized reads
195 as the most abundant 24-nt siRNA position. Further, if other 24-nt siRNA positions
196 possessed a representation level at least half as high as the most abundant 24-nt siRNA
197 position, we also considered these 24-nt siRNA positions as abundant positions.

198

199 **RESULTS**

200 **24-*PHAS* exhibited increased CHH DNA methylation only at the meiotic stage of**
201 **maize anther development**

202 Meiosis is an essential stage in sexual reproduction. To explore if any DNA methylation
203 changes occur before, during, or after meiosis, we performed low-coverage whole genome
204 bisulfite sequencing at three stages of W23 inbred anther development: 0.5 mm anther
205 length (cell proliferation and differentiation), 2.0 mm (prophase I of meiosis), and 4.0 mm
206 (microspore development) anthers (Kelliher & Walbot, 2011) (Fig. **1a-c**; Table **S1**). First,
207 the average levels of CG, CHG, and CHH methylation were determined for each stage
208 (Fig. **1d-f**). The W23 anthers had DNA methylation levels for the CG (75%), CHG (60%),
209 and CHH (2%) contexts that are similar to levels in other inbred lines and tissues
210 examined in previous studies (Li *et al.*, 2014; Zhang *et al.*, 2014). Second, we compared
211 DNA methylation of protein-coding genes, transposons (TEs), and the *PHAS* loci among
212 these three stages. The up- and down-stream regions of protein-coding genes display
213 elevated CHH context DNA methylation at the 2.0 mm stage: about 2-3 times higher than
214 either the 0.5 or 4.0 mm stage (Fig. **1i**). In contrast, there is no major DNA methylation
215 change in the CG and CHG contexts in the gene body regions of protein-coding genes or
216 any contexts for the TEs across the three stages (Fig. **1j**, Fig. **S1c, d, g, h**). Prior work has
217 shown that the 21-nt phasiRNAs peak in abundance by 0.5 mm while the 24-nt
218 phasiRNAs peak at 2.0 mm (Zhai *et al.*, 2015), therefore, we determined if the
219 corresponding *PHAS* loci are differentially methylated at these stages or show any
220 differences relative to protein-coding genes (Fig. **1g, h**, Fig. **S1a, b, e, f**). As with
221 protein-coding genes, no major DNA methylation differences were found in the CG or
222 CHG context across the three stages for either the 21- or 24-*PHAS* loci (Fig. **S1a, b, e, f**).
223 Strikingly, in the CHH context, both 21- and 24-*PHAS* transcribed regions exhibit the
224 highest DNA methylation at 2.0 mm, followed by 0.5 mm; the lowest level occurred at the
225 4.0 mm stage (Fig. **1g, h**).

226 To quantify the stage-specific effects of CHH DNA methylation at various genomic
227 features, we separately analyzed their relative DNA methylation changes compared to the

228 0.5 mm stage (Fig. 1k). All regions analyzed exhibit increased CHH methylation at the 2.0
229 mm stage and reduced CHH methylation at 4.0 mm suggesting dynamic levels of CHH
230 methylation during anther development. Further, we observed that the CHH methylation
231 levels of the transcribed and the up-stream regions of 24-*PHAS* loci, as well as the up- and
232 down-stream regions of protein-coding genes, are more than 50% higher than that of the
233 0.5 mm stage (Fig. 1k). Taken together, these results suggest that 2.0 mm meiotic anthers
234 exhibit distinct CHH DNA methylation patterns and establish that there is developmental
235 regulation of this epigenetic feature.

236 **Elevated CHH DNA methylation of 24-*PHAS* at the meiotic stage is related to the**
237 **presence of 24-nt phasiRNAs**

238 The period of peak DNA methylation at 2.0 mm was investigated further with sequence
239 capture bisulfite-sequencing to enrich for *PHAS* loci. Our main question was whether the
240 elevated CHH DNA methylation on 24-*PHAS* at the 2.0 mm stage depends on the
241 activation of transcription of the loci or on 24-nt phasiRNA abundance. Two male-sterile
242 maize mutants with a profound loss of 24-nt phasiRNAs were utilized. In the *ms23* mutant
243 -- *MS23* encodes a master transcriptional regulator of tapetal development -- few 24-*PHAS*
244 transcripts exist, there are almost no 24-nt phasiRNAs, and *Dcl5* is not expressed (Nan *et*
245 *al.*, 2017). In the downstream *dcl5-1* mutant, 24-*PHAS* transcripts are as high or higher
246 than in the control plants, however, in the absence of DCL5 protein, very few 24-nt
247 phasiRNAs are present (Teng *et al.*, 2020). Analysis of these two mutants can distinguish
248 whether transcriptional activation of the 24-*PHAS* loci or the production of 24-nt
249 phasiRNAs are required for the change in CHH context DNA methylation at 24-*PHAS*
250 loci in 2.0 mm anthers.

251 To pursue the analysis, we generated in-depth, sequence capture bisulfite-sequencing
252 data, as well as sRNA-seq data for 2.0 mm anthers of fully sterile homozygous *dcl5-1*
253 mutants, and the control plants in the T₃ generation (see the Materials and Methods
254 section). In the *dcl5-1* anthers, CG and CHG DNA methylation levels are
255 indistinguishable from control plants (Fig. 2a, b). There was obviously reduced DNA
256 methylation in the CHH context within the transcribed region of 24-*PHAS* loci,

257 particularly 3' of the miRNA cleavage site (CS), in the *dcl5-1* sterile individuals,
258 compared to its control (Fig. 2c). In contrast, 21-*PHAS* loci CHH methylation levels are
259 similar in *dcl5-1* and its control anthers at 2.0 mm (Fig. S2), about 10 days after peak
260 transcript and 21-nt phasiRNA abundances (Zhai *et al.*, 2015). To confirm these results,
261 we generated sequence capture bisulfite-sequencing data from 2.0 mm anthers in T₄
262 generation plants. The substantial CHH methylation difference was present in the
263 transcribed region of 24-*PHAS* loci, but not in the 21-*PHAS* loci in the *dcl5-1* mutant (Fig.
264 S3). Because the sequence capture bisulfite-sequencing data from 2.0 mm anthers in the
265 T₄ generation plants were limited, we did further analysis with data from the T₃ generation
266 plants.

267 In analyzing the sequence capture bisulfite-sequencing data for the 2.0 mm anthers of
268 the *ms23* mutant, we found slightly elevated CG and CHG DNA methylation in the
269 24-*PHAS* transcribed regions in the mutant compared to its fertile control (Fig. 2d, e).
270 Paralleling the results with *dcl5-1*, CHH DNA methylation levels were dramatically
271 reduced 3' of the miR2275-mediated CS across the transcribed region compared to its
272 fertile control (Fig. 2f). In contrast, no major CHH DNA methylation difference was
273 observed at the 21-*PHAS* loci, and CG and CHG DNA methylation levels at these loci
274 were elevated in the mutant as was observed for the 24-*PHAS* loci (Fig. S4). We
275 concluded that these elevated CG and CHG DNA methylation levels in the *ms23* mutant
276 do not compensate for reduced CHH methylation here, because it also occurred in
277 21-*PHAS* loci (without reduced CHH DNA methylation) as well. We propose that absence
278 of the MS23 protein (and failure of tapetal cells to specify and differentiate) affected DNA
279 demethylases required to maintain the CG and CHG methylation in the genome. Because
280 the tapetal cells are such a large fraction (approximately one-third, Kelliher & Walbot,
281 2011) of all anther cells at 2.0 mm, significant changes in this one cell type will show up
282 in whole anther data.

283 Collectively, these data establish that defects in genes required for 24-nt phasiRNA
284 biogenesis result in lower CHH DNA methylation in the corresponding transcribed region
285 of 24-*PHAS* loci, with the most profound impact in the region immediately distal to the

286 miR2275 CS. *ms23* mutants lack both *PHAS* precursors and 24-nt phasiRNAs while
287 *dcl5-1* mutant anthers contain abundant precursors (Teng *et al.*, 2020), but few phasiRNA
288 products. Therefore, we conclude that the elevated CHH DNA methylation of 24-*PHAS*
289 loci at the 2.0 mm stage requires 24-nt phasiRNAs.

290 **Differentially methylated regions in the CHH context at 24-*PHAS* loci**

291 To explore methylation patterns, we identified the CHH-context differentially methylated
292 regions (DMRs) for the *dcl5-1* or *ms23* mutant and their control plants (Table S2; see the
293 Materials and Methods section). For the *dcl5-1* mutant and its control, among 120
294 analyzable 24-*PHAS* loci, we identified *dcl5*-DMRs (DMRs between the *dcl5-1* mutant
295 and its control in the CHH context, abbreviated as *dcl5*-DMRs) from 49 (49/120, 40.8%)
296 24-*PHAS* loci. There were a total of 70 *dcl5*-DMRs at these 49 loci; 19 loci had two or
297 three detected DMRs (Fig. S5). Among 70 *dcl5*-DMRs, 69 of the 70 DMRs display
298 decreased methylation in the *dcl5-1* mutant. In contrast, among 407 analyzable 21-*PHAS*
299 loci, we only identified 34 *dcl5*-DMRs present in 32 (32/407, 6.9%) 21-*PHAS* loci and
300 only two loci had two DMRs; 30 of these DMRs display decreased methylation level in
301 the *dcl5-1* mutant (Fig. S5). Therefore, DMRs involving lower CHH methylation levels,
302 comparing the *dcl5-1* mutant to its controls, are more abundant in the 24-*PHAS* loci than
303 in the 21-*PHAS* loci in 2.0 mm anthers.

304 For the *ms23* mutant and its control there are 96 DMRs located in 68 (68/118, 57.6%)
305 24-*PHAS* loci from 118 analyzable loci; again nearly all are hypomethylated (95/96
306 DMRs) (Table S2). Thirty DMRs were detected (30/398, 7.5%) among 398 analyzable
307 21-*PHAS* loci. There were 22 24-*PHAS* with two or three detected DMRs, and 46 with one
308 DMR, whereas only one DMR was detected in each 21-*PHAS* locus (Fig. S5). In summary,
309 DMRs at 24-*PHAS* loci are more abundant than those found at 21-*PHAS* loci in both the
310 *dcl5-1* and *ms23* mutants.

311 Next, we compared the representation of CHH DMRs in the two mutants. We found 28
312 shared DMRs, 41 *dcl5* specific DMRs, and 67 *ms23* specific DMRs (Fig. 2g, Table S2). If
313 we utilized a lower DMR identification criterion of an absolute methylation change of 2%,

314 then >72% of the DMRs are shared by these mutants. As summarized in the heatmap in
315 Fig. 2g, almost all analyzable DMRs exhibit decreased CHH DNA methylation in both
316 mutants. Further analysis shows, for the shared 28 DMRs, that both the controls of the
317 *dcl5-1* and *ms23* mutant display relatively consistent CHH DNA methylation with the
318 median value of around 10%. In contrast, DMRs restricted to either *dcl5-1* or *ms23* have
319 relatively lower DNA methylation levels with the median value of around 5% in their
320 corresponding fertile controls (Fig. S6). We conclude that the elevated CHH DNA
321 methylation in 2.0 mm control anthers is focused on specific sites in 24-*PHAS* loci and
322 that the extent of CHH methylation depends on the presence of 24-nt phasiRNAs.

323 **CHH DNA methylation at 24-*PHAS* loci normally increases at the meiotic stage**

324 Having established that 24-*PHAS* loci in both *dcl5-1* and *ms23* mutant anthers exhibit low
325 levels of CHH DNA methylation after the CS and across the transcribed gene body at the
326 2.0 mm stage, we sought to distinguish whether this pattern reflected either (i) a failure to
327 maintain higher DNA methylation established at an earlier stage, or (ii) a failure to
328 increase DNA methylation at the 2.0 mm stage. The initial whole genome data presented
329 in Figure 1 established that overall CHH methylation peaked at 2.0 mm. The abundances
330 of 24-nt phasiRNAs from each loci peak at 2.0 mm, with low to moderate level at 1.0 mm,
331 and very low at 0.5 mm (Zhai *et al.*, 2015): transitioning from 0.5 and 1.0 mm there is a
332 slightly increased expression level of 24-nt phasiRNAs, while at the 2.0 mm anther stage
333 there is copious 24-nt phasiRNAs.

334 We generated sequence capture bisulfite-sequencing data for 0.5 and 1.0 mm anthers of
335 the *dcl5-1* mutant and its control (see the Materials and Methods section). First, we
336 compared the methylation patterns for both 21- and 24-*PHAS* in the three developmental
337 stages (0.5, 1.0, and 2.0 mm) from the control plants. No major DNA methylation
338 difference was observed in CG and CHG contexts for either the 21- or 24-*PHAS* across the
339 approximately 10 days of development (Fig. 3a, b, Fig. S7a, b). There was, however, an
340 obvious CHH DNA methylation difference in the transcribed regions of 24-*PHAS* loci 3'
341 of the microRNA CS with relatively low levels in pre-meiotic (0.5 and 1.0 mm) and
342 higher levels in meiotic (2.0 mm) anthers (Fig. 3c); no such difference was observed for

343 21-*PHAS* loci (Fig. S7c). These data clarify that the CHH methylation observed in
344 24-*PHAS* loci in 2.0 mm anthers represents an increase from earlier stages paralleling both
345 normal development and production of 24-nt phasiRNAs. In the *dcl5-1* mutant, CHH
346 methylation levels in the CS to the transcription termination site (TTS) region of 24-*PHAS*
347 loci are nearly constant across the three developmental stages and similar to control
348 anthers at the 0.5 and 1.0 mm stages (Fig. 3c, f). The developmental analysis supports the
349 conclusion that elevated CHH methylation at 24-*PHAS* loci requires the 24-nt phasiRNAs.
350 A parallel analysis of 21-*PHAS* loci identified no obvious DNA methylation differences in
351 any context (Fig. S7d-f).

352 We analyzed CHH DNA methylation patterns of the *dcl5*-DMRs (detected between the
353 *dcl5-1* mutant and its control at the 2.0 mm stage) in the 0.5 and 1.0 mm anthers. Almost
354 all *dcl5*-DMRs showed consistent low levels of CHH DNA methylation across these two
355 stages (Fig. 3g). Collectively, we conclude that the elevated CHH DNA methylation on
356 24-*PHAS* (but not 21-*PHAS*) in the 2.0 mm control anthers is highly related to the burst of
357 24-nt phasiRNAs. Therefore, we conclude that the elevated CHH DNA methylation of
358 24-*PHAS* loci is dependent on the presence of 24-nt phasiRNAs during the period when
359 both transcription of the loci and production of the small RNA products are normally very
360 high in the control anthers.

361 **Abundant phasiRNAs are necessary but not specifically predictive of increased CHH** 362 **DNA methylation at individual 24-*PHAS* loci**

363 There is a low to moderate level of 24-nt phasiRNAs present in 1.0 mm control anthers,
364 with a peak 6 days later at 2.0 mm (Zhai *et al.*, 2015). Despite this, we did not observe an
365 increased CHH DNA methylation level in the 1.0 mm control anthers (Fig. 3c), suggesting
366 that the methylation change requires abundant 24-nt phasiRNAs. We sought to answer the
367 question of whether increased CHH DNA methylation is correlated to the level of 24-nt
368 small RNAs derived from that location. First, we evaluated the CHH DNA methylation
369 level for five 24-*PHAS* subgroups, ranking loci by the levels of 24-nt phasiRNA
370 abundance in the controls of the *dcl5-1* mutant. As shown in Fig. 4a, the median value of
371 the average CHH DNA methylation lowest abundance subgroup is around 3%, while the

372 subsequent 4 subgroups steadily increase from 5% to 9% (Fig. **4a**). Moreover, we found
373 that 24-*PHAS* with *dcl5*-DMRs tend to have a higher level of 24-nt phasiRNAs in control
374 plants (Fig. **S8**).

375 Second, we calculated the CHH DNA methylation levels and small RNA abundance for
376 each 24-*PHAS* locus. Obviously, almost all analyzable 24-*PHAS* loci display relatively
377 elevated CHH DNA methylation in the control plants, and much lower in both *dcl5-1* and
378 *ms23* mutants (Fig. **4b**). Importantly, we also observed that 24-*PHAS* loci with the highest
379 CHH methylation are not the ones with the most abundant 24-nt phasiRNAs (Table **S3**).
380 In other words, the level of CHH methylation at individual 24-*PHAS* loci is not highly
381 correlated with the cumulative abundance of the 24-nt phasiRNA products of that locus.

382 When we investigated the distributions of 24-nt phasiRNA, as well as the *dcl5*- and
383 *ms23*-DMRs, we found that neither the 24-nt phasiRNAs nor the DMRs are evenly
384 distributed. Both show a higher abundance 3' of the microRNA CS (Fig. **S9**). Additionally,
385 a higher proportion of *ms23*-DMRs was seen than of *dcl5*-DMRs across analyzable *PHAS*
386 (Fig. **S9b**), which is consistent with the differential abundance of 24-nt siRNAs on
387 24-*PHAS* in the *ms23* (lower) and *dcl5-1* (higher) mutants (Fig. **4b**).

388 Finally, we examined small RNA and the DNA methylation patterns for individual
389 24-*PHAS* loci in the *dcl5-1* and *ms23* mutants and their controls. Fig. **4c** and Fig. **S10**
390 display two examples: 24-*PHAS*_NO291 (Fig. **4c**) and 24-*PHAS*_NO132 (Fig. **S10**). For
391 24-*PHAS*_NO291, based on the sRNA-seq data, there are two abundant 24-nt phasiRNA
392 positions after the miRNA CS in the controls of both the *dcl5-1* and *ms23* mutants; only a
393 few small RNA reads are detected in the *dcl5-1* mutant, and almost no 24-nt phasiRNAs
394 were present in the *ms23* mutant (Fig. **4c**). Based on the sequence capture
395 bisulfite-sequencing data, it is obvious that the controls possess higher CHH DNA
396 methylation levels across the whole 24-*PHAS* transcript compared to the *dcl5-1* and *ms23*
397 mutants. Three DMRs after the CS were identified in the *dcl5-1* mutant and its control,
398 while another three DMRs were detected in the *ms23* mutant and its control. Two
399 *ms23*-DMRs partially overlap or are adjacent to the three DMRs detected in the *dcl5-1*
400 mutant. And for non-shared *ms23*-DMR regions, the methylation difference was also

401 observed in *dcl5-1* and its control plants. Similar patterns were observed in the
402 24-*PHAS_NO132* (Fig. **S10**).

403 Taken together, the high CHH DNA methylation at 24-*PHAS* requires the presence of
404 24-nt phasiRNAs, but the abundance of 24-nt phasiRNAs is not highly predictive of the
405 CHH methylation level at a *PHAS* locus, although a general low to moderate correlation
406 was observed (Fig. **4a** and Fig. **S11**).

407 **Only one or a few abundant 24-nt phasiRNA(s) accumulate from individual**
408 **24-*PHAS* and likely influence increased CHH DNA methylation**

409 Surprisingly, despite being derived from the same precursor, the abundance of individual
410 24-nt phasiRNAs is highly variable across a locus, similar to the report of
411 non-stoichiometric yield of 21-nt reproductive phasiRNAs from their precursor transcripts
412 (Tamim *et al.*, 2018). The reason for this is unclear: equivalent stoichiometry would be
413 predicted for each 24-nt phasiRNA from the same precursor, but this pattern is not true for
414 any of the expression abundance classes of 24-*PHAS* loci. Therefore, we can investigate
415 within individual loci, whether DMRs are correlated with the abundant 24-nt phasiRNA
416 positions at that locus.

417 To explore as many 24-*PHAS* loci as possible, we re-identified 24-nt phasiRNAs using
418 our newly generated sRNA-seq data of HiII line fertile anthers at the 2.0 mm stage, using
419 the same strategy as previously described (Zhai *et al.*, 2015) (see the Materials and
420 Methods section). As a result, we detected 151 24-*PHAS* loci, 23 of which were newly
421 identified, compared with the list of 24-*PHAS* in the previous study of W23 anthers.
422 Among 176 published 24-*PHAS* in RefB73_v2 in Zhai *et al.* (2015), only 163 of them
423 were evident in RefB73_v4. Among these, only 128 of them were detectable in our
424 sRNA-seq data. Altogether, 186 24-*PHAS* have been detected in different datasets and
425 maize genome assemblies (Zhai *et al.*, 2015 in B73 v4) (Table **S4**).

426 By looking at the 24-nt small RNA distribution across these 24-*PHAS* individually, we
427 found that 24-*PHAS_NO132* and 24-*PHAS_NO291* each had only one or a few highly
428 accumulated 24-nt phasiRNA(s) in the fertile control of the *dcl5-1* mutant (Fig. **4c**, Fig.

429 **S10**). These are not exceptional cases as we observed that all *PHAS* loci tend to possess
430 one or a few highly accumulated 24-nt small RNA type(s), violating the expected
431 stoichiometry from a single precursor. Among 151 expressed 24-*PHAS* loci in our data, 96
432 (63.6%) have only one abundant 24-nt phasiRNA with a super-high accumulation level
433 (35.4 to 1.2 million-fold higher than the lowest accumulated 24-nt type). This is visualized
434 for 24-*PHAS*_NO210 and 24-*PHAS*_NO296 in the fertile control of the *dcl5-1* mutant (Fig.
435 **5a, b**). Another 35 (23.2%) 24-*PHAS* loci have two abundant positions, exemplified by
436 24-*PHAS*_NO173 (Fig. **S12a**), and 20 (13.2%) have three to six abundant positions, as
437 found in 24-*PHAS*_NO203 (Fig. **S12b**).

438 To address if the abundant 24-nt phasiRNA position is well correlated with elevated
439 CHH DNA methylation in 2.0 mm control anthers, we analyzed the methylation
440 distribution across 24-*PHAS* loci. As a result, the average value of the CHH DNA
441 methylation levels of the abundant 24-nt phasiRNA position was 4.6%, while other
442 regions with the lowest expressed 24-nt siRNAs were about 2.3%, and this two-fold
443 difference is highly significant (P value < 0.001 in the Wilcoxon signed-rank test) (Fig.
444 **5e**). The average abundance of small RNAs from abundant position(s) is around 3,200
445 reads per million, more than three orders of magnitude higher than the value of 2 in other
446 regions (Fig. **5f**). Overall, these results indicate that within an individual locus and then
447 collectively in all highly expressed 24-*PHAS* loci, one or a few 24-nt phasiRNAs with
448 high abundance products are most likely resulting in the elevated DNA methylation levels.

449 **Some 24-nt phasiRNAs accumulate in the *dcl5-1* mutant, but not in *ms23* anthers**

450 The *dcl5-1* mutants retain accumulation of some 24-nt small RNAs generated from
451 24-*PHAS* loci (Fig. **S13**). We were curious to know whether these small RNAs are actual
452 phasiRNAs or another class of small RNA. Interestingly, we observed fifty 24-*PHAS* loci
453 with 24-nt siRNAs generated in an obvious phasing pattern by manual check (phasing
454 score greater than 15, and passing our manual check, see the Materials and Methods
455 section) (Table **S5**). Compared to fertile anthers, however, the accumulation of these
456 phasiRNAs was 73-fold lower in *dcl5-1* mutants at 2.0 mm. Therefore, other DCLs,
457 perhaps DCL3 given its propensity to process heterochromatic siRNAs into 24 nt lengths,

458 substitute by slicing the abundant precursor transcripts, albeit inefficiently, when DCL5 is
459 absent (Teng *et al.*, 2020). In the *ms23* mutant, none of the detected 24-nt small RNAs
460 exhibited a phasing pattern, as expected because there is no detectable expression of
461 24-*PHAS* loci.

462 Two representative examples of the distribution of 24-nt small RNAs in the 2.0 mm
463 *dcl5-1* mutants are displayed in Fig. 5. Notably, only one 24-nt small RNA with highly
464 abundant accumulation is present in 24-*PHAS*_NO296 and another in 24-*PHAS*_NO210.
465 In both cases, these map 3' of the miR2275 CS (Fig. 5a, b). Other 24-nt small RNAs
466 (minor peaks) from these two 24-*PHAS* loci have relatively low accumulation levels.
467 Importantly, the 24-nt siRNAs from 24-*PHAS*_NO296 exhibited a clear phased pattern in
468 the *dcl5-1* mutant (phasing score greater than 25), whereas 24-*PHAS*_NO210 24-nt RNAs
469 were not in a phased pattern (Fig. 5c, d). Consequently, some 24-*PHAS* loci generate
470 24-nt siRNAs independently of the usual biogenesis of phasiRNAs.

472 **Discussion**

473 This study sought to further explore the hypothesis that 24-nt phasiRNAs can impact
474 DNA methylation at their cognate loci, a type of *cis* regulation (Dukowic-Schulze *et al.*,
475 2016). We first demonstrated that CHH DNA methylation levels are developmentally
476 regulated, being highest in 2.0 mm, mid-meiosis anthers compared to earlier or later stages.
477 In fertile anthers, CHH DNA methylation levels increase significantly at 2.0 mm, the stage
478 of peak 24-nt phasiRNA abundance. To distinguish whether transcriptional activation of
479 24-*PHAS* loci or the 24-nt phasiRNA products contribute to the observed CHH DNA
480 methylation increase, we analyzed two mutants: *ms23*, in which transcriptional activation
481 of the 24-*PHAS* loci fails to occur, and *dcl5-1*, in which transcript abundance is nearly
482 normal (Fig. S14), but far fewer 24-nt phasiRNA products exist. Both *ms23* and *dcl5-1*
483 mutants failed to exhibit the elevated CHH methylation at the 24-*PHAS* loci found at 2.0
484 mm in normal anthers, suggesting that 24-nt phasiRNAs are necessary to direct increased
485 CHH DNA methylation at this developmental stage. Further support for a role of 24-nt
486 phasiRNAs in modulating CHH DNA methylation is provided by the observation that
487 elevated CHH DNA methylation of each 24-*PHAS* locus requires the abundant 24-nt small
488 RNA derived from that 24-*PHAS*. Additionally, within a locus, there is enormous
489 variation in the abundance of individual 24-nt phasiRNAs despite derivation from a
490 common precursor; this matches observations from 21-*PHAS* loci (Tamim *et al.*, 2018).
491 The CHH DNA methylation level of the abundant 24-nt phasiRNA position is obviously
492 higher than that at the genomic positions corresponding to low abundance 24-nt siRNAs
493 across the locus (Fig. 5e, f). Collectively, these three lines of evidence support the idea
494 that 24-nt phasiRNAs can direct increased CHH DNA methylation in *cis*.

495 In whole anthers, the detectable changes in DNA methylation will be from the abundant
496 somatic cells, not the meiocytes. The tapetum synthesizes 24-nt phasiRNAs (Zhai *et al.*,
497 2015; Teng *et al.*, 2020) and both the *ms23* and *dcl5-1* mutants impact tapetal
498 development. Therefore, we propose that the CHH DNA methylation changes we
499 quantified reflect events in the tapetum. As CHH DNA methylation flanking genes
500 exhibits a positive relationship to gene expression (Gent *et al.*, 2013), we speculate that

501 the presumably tapetal CHH DNA methylation might regulate expression of these *PHAS*
502 loci (up or down) or help with chromatin compaction or binucleation of tapetal cells.

503 A reasonable question is whether *cis*-directed enhancement of methylation is the actual
504 or only function of 24-nt reproductive phasiRNAs. It seems somewhat unlikely, as it
505 would represent a closed circuit: highly expressed 24-nt phasiRNAs -> high CHH
506 methylation --> increase of PHAS transcription. At a minimum, our results do
507 demonstrate that 24-nt phasiRNAs are competent to direct CHH DNA methylation. This
508 could result from mis-loading, in an abundance-dependent manner into AGO4, the
509 Argonaute typically loaded with 24-nt heterochromatic siRNAs to direct DNA
510 methylation (Zilberman *et al.*, 2003). Like the observations described here, 21-nt
511 reproductive phasiRNAs in rice and maize have been shown and validated to function in
512 *cis* to direct slicing of their own precursors (Tamim *et al.*, 2018). But it is unclear also in
513 that case if this *cis* activity is the primary function of the phasiRNAs or an unintended
514 consequence of highly abundant small RNAs misloaded into the ‘wrong’ AGO protein.
515 Until we know the precise functions of 24-nt reproductive phasiRNAs, the AGO proteins
516 into which they are loaded, and their predominant targets if any exist, the importance of
517 the *cis*-directed DNA methylation reported here may remain unclear.

519 **Acknowledgments**

520 The seeds of *dcl5-1* and *ms23* mutants were generously provided by Han Zhang and
521 Guo-ling Nan, respectively. We thank Peter Hermanson for the preparation of sequence
522 capture bisulfite-sequencing libraries and Sandra Mathioni for small RNA-seq libraries.
523 This work was supported by U.S. National Science Foundation Plant Genome Research
524 Program (NSF-PGRP) award #1649424 (B.C.M. and V.W.), the International Postdoctoral
525 Exchange Fellowship Program award #20140067 (M.Z.), U. S. National Science
526 Foundation Grants DBI-1237931 (N.M.S), and Starting Funding of the Chinese Academy
527 of Sciences (Y971RG1001 to M.Z.). Requests for materials should be addressed to
528 walbot@stanford.edu. Raw data were submitted to NCBI's Short Read Archive under
529 BioProject accession PRJNA639640.

530 **Author contributions**

531 M.Z. and V.W. conceived of the project; M.Z. performed experiments of the project as
532 part of M.Z.'s postdoctoral training at Stanford University; X.M., C.W., and Q.L.
533 analyzed sequencing data and built graphs; M.Z. and V.W. wrote the manuscript with
534 editing by B.C.M., N.M.S., and with input from all co-authors. MZ, XM and VW
535 contributed equally to this work.

537 **References**

- 538 **Allen E, Xie Z, Gustafson AM, Carrington JC. 2005.** MicroRNA-directed phasing during
539 *trans-acting* siRNA biogenesis in plants. *Cell* **121**: 207–221.
- 540 **Aravin AA, Hannon GJ, Brennecke J. 2007.** The piwi-piRNA pathway provides an adaptive
541 defense in the transposon arms race. *Science* **318**: 761–764.
- 542 **Arikit S, Zhai J, Meyers BC. 2013.** Biogenesis and function of rice small RNAs from non-coding
543 RNA precursors. *Current Opinion in Plant Biology* **16**: 170–179.
- 544 **Borges F, Martienssen RA. 2015.** The expanding world of small RNAs in plants. *Nature Reviews*
545 *Molecular Cell Biology* **16**: 727–741.
- 546 **Chen S, Zhou Y, Chen Y, Gu J. 2018.** fastp: an ultra-fast all-in-one FASTQ preprocessor.
547 *Bioinformatics* **34**: i884–i890.
- 548 **De Paoli E, Dorantes-Acosta A, Zhai J, Accerbi M, Jeong DH, Park S, Meyers BC, Jorgensen**
549 **RA, Green PJ. 2009.** Distinct extremely abundant siRNAs associated with cosuppression in petunia.
550 *RNA* **15**: 1965–1970.
- 551 **Deng P, Muhammad S, Cao M, Wu L. 2018.** Biogenesis and regulatory hierarchy of phased small
552 interfering RNAs in plants. *Plant Biotechnology Journal* **16**: 965–975.
- 553 **Dukowic-Schulze S, Sundararajan A, Ramaraj T, Kianian S, Pawlowski WP, Mudge J, Chen C.**
554 **2016.** Novel meiotic miRNAs and indications for a role of phasiRNAs in meiosis. *Frontiers in Plant*
555 *Science* **7**: 762.
- 556 **Fan Y, Yang J, Mathioni SM, Yu J, Shen J, Yang X, Wang L, Zhang Q, Cai Z, Xu C, et al. 2016.**
557 *PMSIT*, producing phased small-interfering RNAs, regulates photoperiod-sensitive male sterility in
558 rice. *Proceedings of the National Academy of Sciences of the United States of America* **113**: 15144–
559 15149.
- 560 **Fei Q, Yang L, Liang W, Zhang D, Meyers BC. 2016.** Dynamic changes of small RNAs in rice
561 spikelet development reveal specialized reproductive phasiRNA pathways. *Journal of Experimental*
562 *Botany* **67**: 6037–6049.

-
- 563 **Fu Q, Wang PJ. 2014.** Mammalian piRNAs: Biogenesis, function, and mysteries. *Spermatogenesis* **4**:
564 e27889.
- 565 **Gent JI, Ellis NA, Guo L, Harkess AE, Yao Y, Zhang X, Dawe RK. 2013.** CHH islands: De novo
566 DNA methylation in near-gene chromatin regulation in maize. *Genome Research* **23**: 628–637.
- 567 **Girard A, Sachidanandam R, Hannon GJ, Carmell MA. 2006.** A germline-specific class of small
568 RNAs binds mammalian Piwi proteins. *Nature* **442**: 199–202.
- 569 **Grivna ST, Beyret E, Wang Z, Lin H. 2006.** A novel class of small RNAs in mouse spermatogenic
570 cells. *Genes and Development* **20**: 1709–1714.
- 571 **Han Z, Crisp PA, Stelpflug S, Kaeppler SM, Li Q, Springer NM. 2018.** Heritable epigenomic
572 changes to the Maize methylome resulting from tissue culture. *Genetics* **209**: 983–995.
- 573 **Han BW, Wang W, Li C, Weng Z, Zamore PD. 2015.** PiRNA-guided transposon cleavage initiates
574 Zucchini-dependent, phased piRNA production. *Science* **348**: 817–821.
- 575 **Huang X, Zhang S, Li K, Thimmapuram J, Xie S. 2018.** ViewBS: A powerful toolkit for
576 visualization of high-throughput bisulfite sequencing data. *Bioinformatics* **34**: 708–709.
- 577 **Jiao Y, Peluso P, Shi J, Liang T, Stitzer MC, Wang B, Campbell MS, Stein JC, Wei X, Chin CS
578 et al. 2017.** Improved maize reference genome with single-molecule technologies. *Nature* **546**: 524–
579 527.
- 580 **Johnson C, Kasprzewska A, Tennessen K, Fernandes J, Nan GL, Walbot V, Sundaresan V,
581 Vance V, Bowman LH. 2009.** Clusters and superclusters of phased small RNAs in the developing
582 inflorescence of rice. *Genome Research* **19**: 1429–1440.
- 583 **Kakrana A, Mathioni SM, Huang K, Hammond R, Vandivier L, Patel P, Arikrit S, Shevchenko
584 O, Harkess AE, Kingham B et al. 2018.** Plant 24-nt reproductive phasiRNAs from intramolecular
585 duplex mRNAs in diverse monocots. *Genome Research* **28**: 1333–1344.
- 586 **Kelliher T, Walbot V. 2011.** Emergence and patterning of the five cell types of the *Zea mays* anther
587 locule. *Developmental Biology* **350**: 32–49.
- 588 **Kim D, Langmead B, Salzberg SL. 2015.** HISAT: a fast spliced aligner with low memory
589 requirements. *Nature Methods* **12**: 357–360.

590 **Langmead B, Trapnell C, Pop M, Salzberg SL. 2009.** Ultrafast and memory-efficient alignment of
591 short DNA sequences to the human genome. *Genome Biology* **10**:R25.

592 **Le Thomas A, Rogers AK, Webster A, Marinov GK, Liao SE, Perkins EM, Hur JK, Aravin AA,**
593 **Tóth KF. 2013.** Piwi induces piRNA-guided transcriptional silencing and establishment of a
594 repressive chromatin state. *Genes and Development* **27**: 390–399.

595 **Li Q, Eichten SR, Hermanson PJ, Zaunbrecher VM, Song J, Wendt J, Rosenbaum H, Madzima**
596 **TF, Sloan AE, Huang J et al. 2014.** Genetic perturbation of the maize methylome. *Plant Cell* **26**:
597 4602–4616.

598 **Liu L, Ren S, Guo J, Wang Q, Zhang X, Liao P, Li S, Sunkar R, Zheng Y. 2018.** Genome-wide
599 identification and comprehensive analysis of microRNAs and phased small interfering RNAs in
600 watermelon. *BMC Genomics* **19**(Suppl 2):111.

601 **Luteijn MJ, Ketting RF. 2013.** PIWI-interacting RNAs: From generation to transgenerational
602 epigenetics. *Nature Reviews Genetics* **14**: 523–534.

603 **Mathioni SM, Kakrana A, Meyers BC. 2017.** Characterization of plant small RNAs by next
604 generation sequencing. *Current Protocols in Plant Biology* **2**: 39–63.

605 **Mohn F, Handler D, Brennecke J. 2015.** PiRNA-guided slicing specifies transcripts for
606 Zucchini-dependent, phased piRNA biogenesis. *Science* **348**: 812–817.

607 **Nan GL, Zhai J, Arikiti S, Morrow D, Fernandes J, Mai L, Nguyen N, Meyers BC, Walbot V.**
608 **2017.** MS23, a master basic helix-loop-helix factor, regulates the specification and development of the
609 tapetum in maize. *Development* **144**: 163–172.

610 **Ono S, Liu H, Tsuda K, Fukai E, Tanaka K, Sasaki T, Nonomura K. 2018.** EAT1 transcription
611 factor, a noncell-autonomous regulator of pollen production, activates meiotic small RNA biogenesis
612 in rice anther tapetum. *PLoS Genetics* **14**: e1007238.

613 **Pertea M, Pertea GM, Antonescu CM, Chang T-C, Mendell JT, Salzberg SL. 2015.** StringTie
614 enables improved reconstruction of a transcriptome from RNA-seq reads. *Nature Biotechnology* **33**:
615 290–295.

-
- 616 **Rajagopalan R, Vaucheret H, Trejo J, Bartel DP. 2006.** A diverse and evolutionarily fluid set of
617 microRNAs in *Arabidopsis thaliana*. *Genes & Development* **20**: 3407–3425.
- 618 **Schultz MD, Schmitz RJ, Ecker JR. 2012.** ‘Leveling’ the playing field for analyses of single-base
619 resolution DNA methylomes. *Trends in Genetics* **28**: 583–585.
- 620 **Shuai P, Su Y, Liang D, Zhang Z, Xia X, Yin W. 2016.** Identification of phasiRNAs and their
621 drought- responsiveness in *Populus trichocarpa*. *FEBS Letters* **590**: 3616–3627.
- 622 **Song X, Li P, Zhai J, Zhou M, Ma L, Liu B, Jeong DH, Nakano M, Cao S, Liu C et al. 2012a.**
623 Roles of DCL4 and DCL3b in rice phased small RNA biogenesis. *Plant Journal* **69**: 462–474.
- 624 **Song X, Wang D, Ma L, Chen Z, Li P, Cui X, Liu C, Cao S, Chu C, Tao Y et al. 2012b.** Rice
625 RNA-dependent RNA polymerase 6 acts in small RNA biogenesis and spikelet development. *Plant*
626 *Journal* **71**: 378–389.
- 627 **Tamim S, Cai Z, Mathioni SM, Zhai J, Teng C, Zhang Q, Meyers BC. 2018.** *Cis*-directed
628 cleavage and nonstoichiometric abundances of 21-nucleotide reproductive phased small interfering
629 RNAs in grasses. *New Phytologist* **220**: 865–877.
- 630 **Teng C, Zhang H, Hammond R, Huang K, Meyers BC, Walbot V. 2020.** *Dicer-like 5* deficiency
631 confers temperature-sensitive male sterility in maize. *Nature Communications* **11**: 2912.
- 632 **Urich MA, Nery JR, Lister R, Schmitz RJ, Ecker JR. 2015.** MethylC-seq library preparation for
633 base-resolution whole-genome bisulfite sequencing. *Nature Protocols* **10**: 475–483.
- 634 **Vagin V V, Sigova A, Li C, Seitz H, Gvozdev V, Zamore PD. 2006.** A distinct small RNA pathway
635 silences selfish genetic elements in the germline. *Science* **313**: 320 – 324.
- 636 **Wu L. 2013.** DICER-LIKE1 processed *trans-acting* siRNAs mediate DNA methylation: Case study
637 of complex small RNA biogenesis and action pathways in plants. *Plant Signaling & Behavior* **8**:
638 e22476.
- 639 **Wu L, Mao L, Qi Y. 2012.** Roles of DICER-LIKE and ARGONAUTE proteins in *TAS*-derived small
640 interfering RNA-triggered DNA methylation. *Plant Physiology* **160**: 990–999.

641 **Xi Y, Li W. 2009.** BSMAP: Whole genome bisulfite sequence MAPping program. *BMC*
642 *Bioinformatics* **10**: 232.

643 **Xia R, Chen C, Pokhrel S, Ma W, Huang K, Patel P, Wang F, Xu J, Liu Z, Li J et al. 2019.** 24-nt
644 reproductive phasiRNAs are broadly present in angiosperms. *Nature Communications* **10**: 627.

645 **Xia R, Xu J, Arikiti S, Meyers BC. 2015.** Extensive families of miRNAs and *PHAS* loci in Norway
646 spruce demonstrate the origins of complex phasiRNA networks in seed plants. *Molecular Biology and*
647 *Evolution* **32**: 2905–2918.

648 **Yu Y, Zhou Y, Zhang Y, Chen Y. 2018.** Grass phasiRNAs and male fertility. *Science China Life*
649 *Sciences* **61**: 148–154.

650 **Zhai J, Zhang H, Arikiti S, Huang K, Nan GL, Walbot V, Meyers BC. 2015.** Spatiotemporally
651 dynamic, cell-type–dependent premeiotic and meiotic phasiRNAs in maize anthers. *Proceedings of*
652 *the National Academy of Sciences of the United States of America* **112**: 3146–3151.

653 **Zhang M, Xie S, Dong X, Zhao X, Zeng B, Chen J, Li H, Yang W, Zhao H, Wang G et al. 2014.**
654 Genome-wide high resolution parental-specific DNA and histone methylation maps uncover patterns
655 of imprinting regulation in maize. *Genome Research* **24**: 167–176.

656 **Zilberman D, Cao X, Jacobsen SE. 2003.** ARGONAUTE4 control of locus-specific siRNA
657 accumulation and DNA and histone methylation. *Science* **299**: 716–719.

658

660 **Figure legends**

661 **Figure 1. 24-*PHAS* loci display stage-specific DNA methylation patterns during maize anther**
662 **development.**

663 (a) to (c) Transverse sections of maize anthers at three length stages: 0.5 mm, cell proliferation and
664 differentiation (a); 2.0 mm, prophase I of meiosis (b); 4.0 mm, binucleate gametophyte (c).
665 Abbreviations: AR, archesporial cell(s); Mei, meiocytes; Msp, microspore; SPC, secondary parietal
666 cell(s); T, tapetum; ML, middle layer; EN, endothecium; E, Epidermis. Bars = 30 μ m. (d) to (f)
667 Genome-wide DNA methylation levels in the CG (a), CHG (b), and CHH (c) contexts at three stages.
668 Y axis shows the average CG DNA methylation level (d), CHG methylation level (e), and CHH
669 methylation level (f). (g) to (j) CHH DNA methylation profiles in the transcribed regions and 2 kb
670 before and 2 kb after the 21-*PHAS* loci (g), 24-*PHAS* loci (h), protein-coding genes (i), and
671 transposons (TEs) (j). Y axis is the CHH methylation level (g-j). From (g) to (j), TSS indicates the
672 transcription start site, and TTS indicates the transcription termination site. (k) Percentage change in
673 CHH methylation levels of 2.0 and 4.0 mm anthers compared to the 0.5 mm stage at the 21-*PHAS*,
674 24-*PHAS*, protein-coding genes, and TEs, calculated as level in percent at 2.0 mm - 0.5 mm and 4.0
675 mm - 0.5 mm. Y axis displays the resulting % change relative to the 0.5 mm stage. From (d) to (k),
676 fertile anthers were dissected from the W23 inbred, and low-coverage whole genome bisulfite
677 sequencing data were used.

679 **Figure 2. DNA methylation levels at 24-PHAS loci in the *dcl5-1* and *ms23* mutants compared to**
680 **their control plants at the 2.0 mm stage of maize anthers.**

681 These deep coverage data were generated using a sequence capture bisulfite-sequencing
682 strategy. (a) to (c) Plots of the three context methylation profiles at 24-PHAS in the *dcl5-1*
683 mutant (blue line) and the control plants (red line). (d) to (f) Alterations in the methylation
684 profiles at 24-PHAS in the *ms23* mutant (purple line) and its control plants (gold line).
685 From (a) to (f), TSS indicates the transcription start site, CS indicates the microRNA
686 cleavage site in the precursor RNA transcript, and TTS indicates the transcription
687 termination site. MS (*dcl5*) and MS (*ms23*) indicates the male sterile *dcl5-1* or *ms23*
688 mutant, while F (*dcl5*) and F (*ms23*) represents the controls for *dcl5-1* and *ms23* mutants.
689 Under the p-value < 0.001 as threshold, the significant bins were highlighted in grey
690 background in (c) and (f). Only PHAS loci (N = 117 ~ 120, different numbers for each plot)
691 with >5 mapped reads were used for calculation, and the methylation level of each bin was
692 calculated using the weighted DNA methylation computing method ($\#C/(\#C+\#T)$)
693 (Schultz *et al.*, 2012). (g) Heatmap plot of CHH DNA methylation levels for the
694 *dcl5*-Differentially Methylated Regions (DMRs identified between the *dcl5-1* mutant and
695 its control plants) and *ms23*-DMRs (DMRs identified between the *ms23* mutant and its
696 control plants). All DMRs identified in 24-PHAS loci were included in this analysis. The
697 label changing from white to dark blue color indicates increasing CHH methylation (%).
698 MS refers to male-sterile mutants, and F refers to the control plants.

700 **Figure 3. DNA methylation levels at 24-PHAS loci in the *dcl5-1* mutant and its**
701 **control plants in maize pre-meiotic (0.5 and 1.0 mm), and meiotic 2.0 mm anthers.**

702 Deep coverage data were generated using the sequence capture bisulfite-sequencing
703 strategy. (a) to (c) Plot of the three context methylation profiles at 24-PHAS loci in the
704 control plants of the *dcl5-1* mutant in 0.5 (orange line), 1.0 (purple line), and 2.0 mm (red
705 line) stage anthers. (d) to (f) Plot of the three context methylation profiles at 24-PHAS loci
706 in the *dcl5-1* mutant in the 0.5 (light green line), 1.0 (pink line), and 2.0 mm (light blue
707 line) stage anthers. From (a) to (f), plots were compiled using the same strategy as
708 described for Fig. 2a-f. TSS, transcription start site; CS, the miR2275 cleavage site in the
709 precursor RNA transcript; and TTS, transcription termination site. Under the p-value <
710 0.001 as threshold, the significant bins were highlighted in grey background (between 1.0
711 and 2.0 mm) and orange background (between 0.5 and 2.0 mm) (g) Heatmap plot of CHH
712 DNA methylation levels for the *dcl5*-DMRs identified between the *dcl5-1* mutant and its
713 control plants at the 2.0 mm stage at all three stages. The label changing from white to
714 dark blue color indicates increasing CHH methylation (%). MS refers to male-sterile, and
715 F refers to control plants.

717 **Figure 4. High CHH DNA methylation at 24-PHAS loci requires abundant 24-nt**
718 **small RNAs in maize.**

719 **(a)** CHH DNA methylation levels of 5 subgroups of 24-PHAS with different levels of
720 small RNA abundance in the control plants of the *dcl5-1* mutant. All detected 151
721 24-PHAS loci were divided into 5 subgroups, with their phasiRNA abundance ranging
722 from 10^2 to 10^3 , 10^3 to 10^4 , 10^4 to 10^5 , 10^5 to 10^6 , and 10^6 to 10^7 reads. Correspondingly,
723 the number of analyzable 24-PHAS loci is 8, 24, 51, 48, and 10, while the numbers of
724 un-analyzable examples are 2, 4, 3, 1, and 0. The CHH DNA methylation level was
725 calculated by weighted DNA methylation for two adjacent 50 bp windows with the
726 highest CHH DNA methylation level at the PHAS. MS indicates the *dcl5-1* or *ms23*
727 mutant, while F (*dcl5*) and F (*ms23*) represent the control plants for *dcl5-1* and *ms23*
728 mutants. Boxplot encloses the 25 - 75th percentiles (interquartile range); bold black line is
729 the median; the whiskers refer to values greater than interquartile range excluding outliers;
730 black dots refer to outliers. **(b)** Heatmap of 24-nt small RNA abundance calculated by
731 reads per million (RPM, blue scale) and CHH DNA methylation levels (red) for each
732 analyzable 24-PHAS (N = 120). The expression level of 24-nt phasiRNAs in the *ms23*
733 mutant and its control was calculated based on the published sRNA-seq data from Zhai et
734 al., 2015. The control for *dcl5-1* shows the loci ranked by DNA methylation level, and the
735 other seven rows correspond to this order. **(c)** A view of 24-nt small RNA and CHH DNA
736 methylation patterns in control plants and two mutants across 24-PHAS_NO291 locus and
737 flanking 200 bp regions. The top four graphs display the 24-nt siRNA abundance with
738 discontinuous line by reads per million (RPM), while the bottom four graphs show the
739 CHH DNA methylation percent in analyzable windows at PHAS loci. Each gray box
740 indicates a *dcl5*- or *ms23*-DMR. Dotted lines indicate the microRNA cleavage site.
741 Vertical gray bars represent 24 nt spacing.

742

744 **Figure 5. PhasiRNA abundances, CHH DNA methylation, and phased patterns**
745 **across the 24-PHAS_NO210 and 24-PHAS_NO296 loci in four genotypes at the 2.0**
746 **mm stage of maize anthers.**

747 **(a-b)** phasiRNA abundance across the loci 24-PHAS_NO210 **(a)** and 24-PHAS_NO296 **(b)**
748 in the *dcl5-1* and *ms23* mutant, and their controls. **(c-d)** Phased patterns at
749 24-PHAS_NO210 **(c)** and 24-PHAS_NO296 **(d)** in the *dcl5-1* and *ms23* mutant, and their
750 controls. Dotted lines indicate the microRNA cleavage site. Vertical gray bars represent
751 24 nt spacing. MS indicates the *dcl5-1* or *ms23* mutant, while F (*dcl5*) and F (*ms23*)
752 represent the control plants for *dcl5-1* and *ms23* mutants. **(e)** Comparison of CHH DNA
753 methylation of the abundant 24-nt phasiRNA positions (this corresponds to the peak
754 region with super highly expressed 24-nt phasiRNA(s)) and other regions (with no or
755 lowly expressed 24-nt phasiRNAs) at the 24-PHAS. One hundred and forty 24-PHAS loci
756 were used here. **(f)** Comparison of 24-nt small abundance from the abundant 24-nt
757 phasiRNA positions and other regions on 24-PHAS loci. Boxplot encloses the 25 - 75th
758 percentiles (interquartile range); bold black line is the median; the whiskers refer to values
759 greater than interquartile range excluding outliers; black dots refer to outliers. One
760 hundred and fifty-one 24-PHAS loci were used here.
761

Supporting Information

Fig S1. CG and CHG DNA methylation profiles in the transcribed regions and 2 kb before and 2 kb after the 21-*PHAS*, 24-*PHAS*, protein-coding genes, and transposons (TEs).

Fig S2. DNA methylation levels across the 21-*PHAS* transcribed regions and flanking 200 bp regions in the CG, CHG, and CHG contexts at the 2.0 mm stage of the *dcl5-1* mutants (MS) and its controls (F) in a family segregating 3:1 for sterile individuals.

Fig S3. DNA methylation levels at 24-*PHAS* and 21-*PHAS* transcribed regions and flanking 200 bp regions in 2.0 mm anthers.

Fig S4. DNA methylation levels within the transcribed regions and flanking 200 bp regions of 381 to 400 21-*PHAS* loci (analyzed based on presence in a dataset) in the CG, CHG, and CHG contexts in 2.0 mm anthers.

Fig S5. Differentially methylated region (DMR) counts at 24-*PHAS* and 21-*PHAS* loci with *dcl5*- or *ms23*-DMRs at the 2.0 mm stage.

Fig S6. CHH DNA methylation distribution of DMRs specific to *dcl5-1* mutant, shared by *dcl5-1* and *ms23* samples, and *ms23*-specific DMRs.

Fig S7. DNA methylation levels at 21-*PHAS* loci in the *dcl5-1* mutant and its control in pre-meiotic (0.5 and 1.0 mm), and meiotic 2.0 mm anthers.

Fig S8. Comparison of 24-nt phasiRNA abundance for 49 24-*PHAS* with *dcl5*-DMR(s) and 71 24-*PHAS* without detectable DMR(s).

Fig S9. Distribution of 24-nt small RNAs and 24-*PHAS* with *dcl5*- or *ms23*-DMRs across 24-*PHAS* loci plus the 200 bp flanking regions in the *dcl5-1* and *ms23* mutants and their fertile controls.

Fig S10. A view of 24-nt small RNA and CHH DNA methylation patterns in two mutants, *dcl5-1* and *ms23*, and their fertile controls across locus 24-*PHAS*_NO132 and its 200 bp flanking regions.

Fig S11. Correlation between the abundance of 24-nt phasiRNAs and CHH methylation level at 24-*PHAS*.

Fig S12. 24-nt small RNA distribution plotted across the transcribed regions of the 24-*PHAS*_NO173 and 24-*PHAS*_NO203 loci in the control (F) of the *dcl5-1* mutant at the 2.0 mm stage.

Fig S13. Abundance of 24-nt phasiRNAs from 151 24-*PHAS* loci in the 2.0 mm anthers.

Fig S14. The expression levels of all 24-*PHAS* loci in the two replicates of the *dcl5-1* mutants and its control plants.

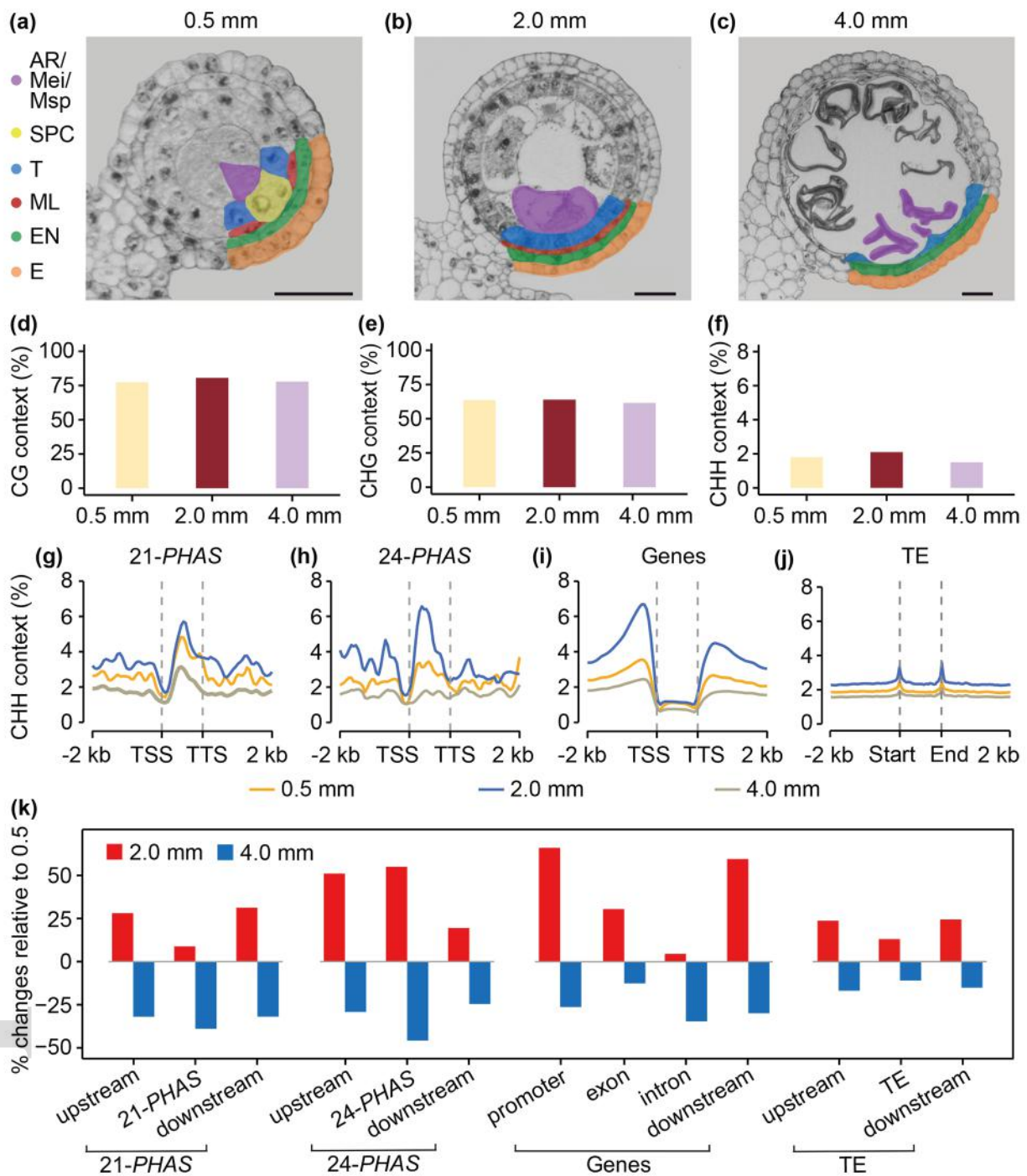
Table S1. Summary of whole genome bisulfite sequencing, sequence capture bisulfite-sequencing, sRNA-seq, and RNA-seq libraries newly generated in this study.

Table S2. CHH DNA methylation levels of each *dcl5*- and *ms23*-DMR in the 2.0 mm *dcl5-1* and *ms23* mutants and their fertile controls.

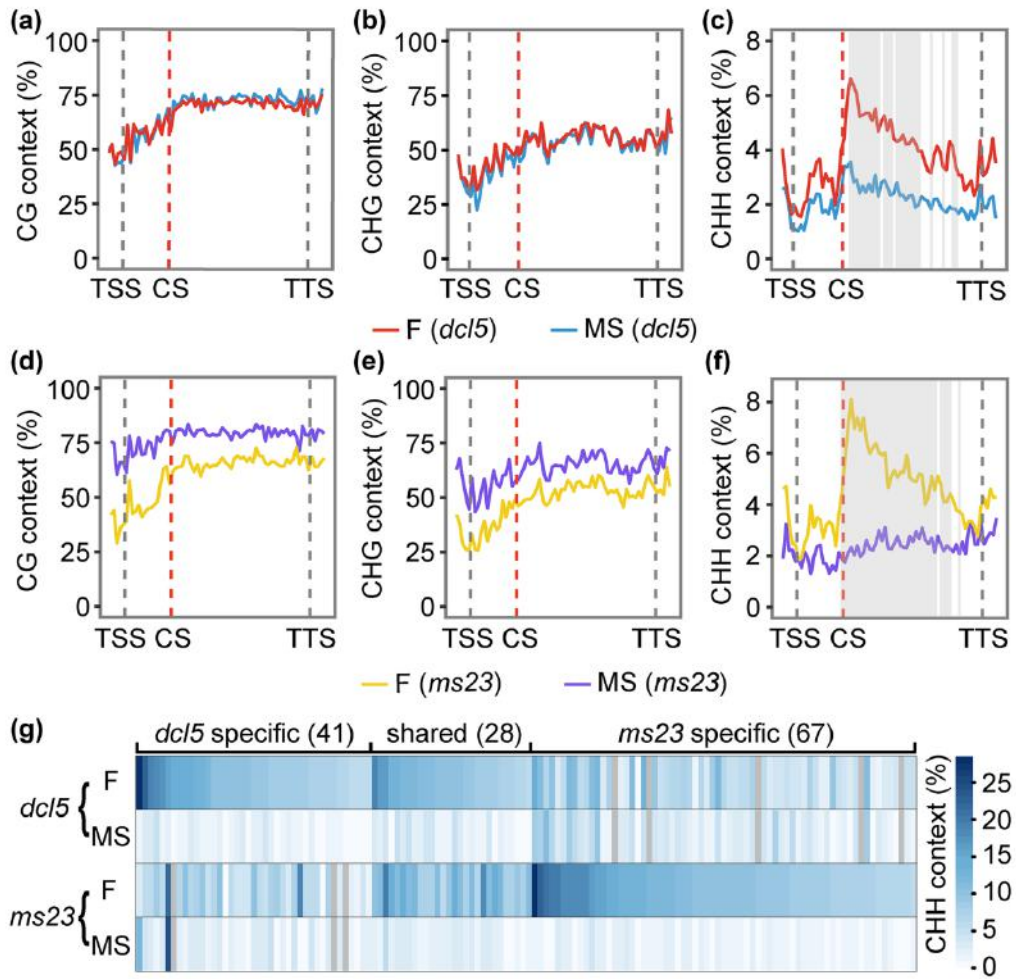
Table S3. 24-nt sRNA abundance and CHH methylation level of analyzable 24-*PHAS* loci.

Table S4. Updated list of 186 24-*PHAS* in maize (RefB73_v4) with the 24-nt small RNA abundance calculated by reads per million (RPM) on each locus in the four genotypes.

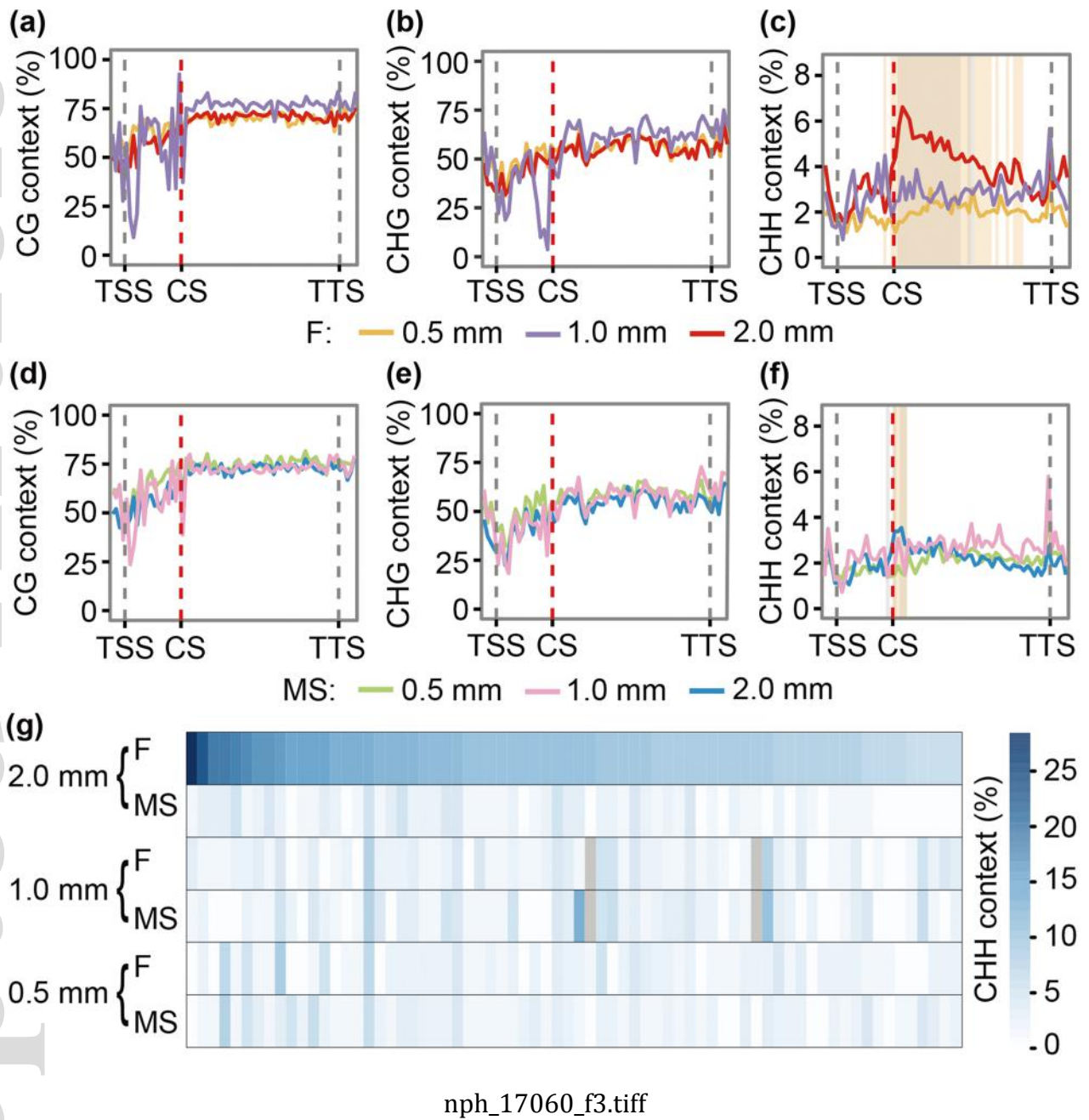
Table S5. The largest phasing score of certain 24-nt phasiRNA on each 24-*PHAS* in the *dcl5-1* and *ms23* mutants, as well as their controls.

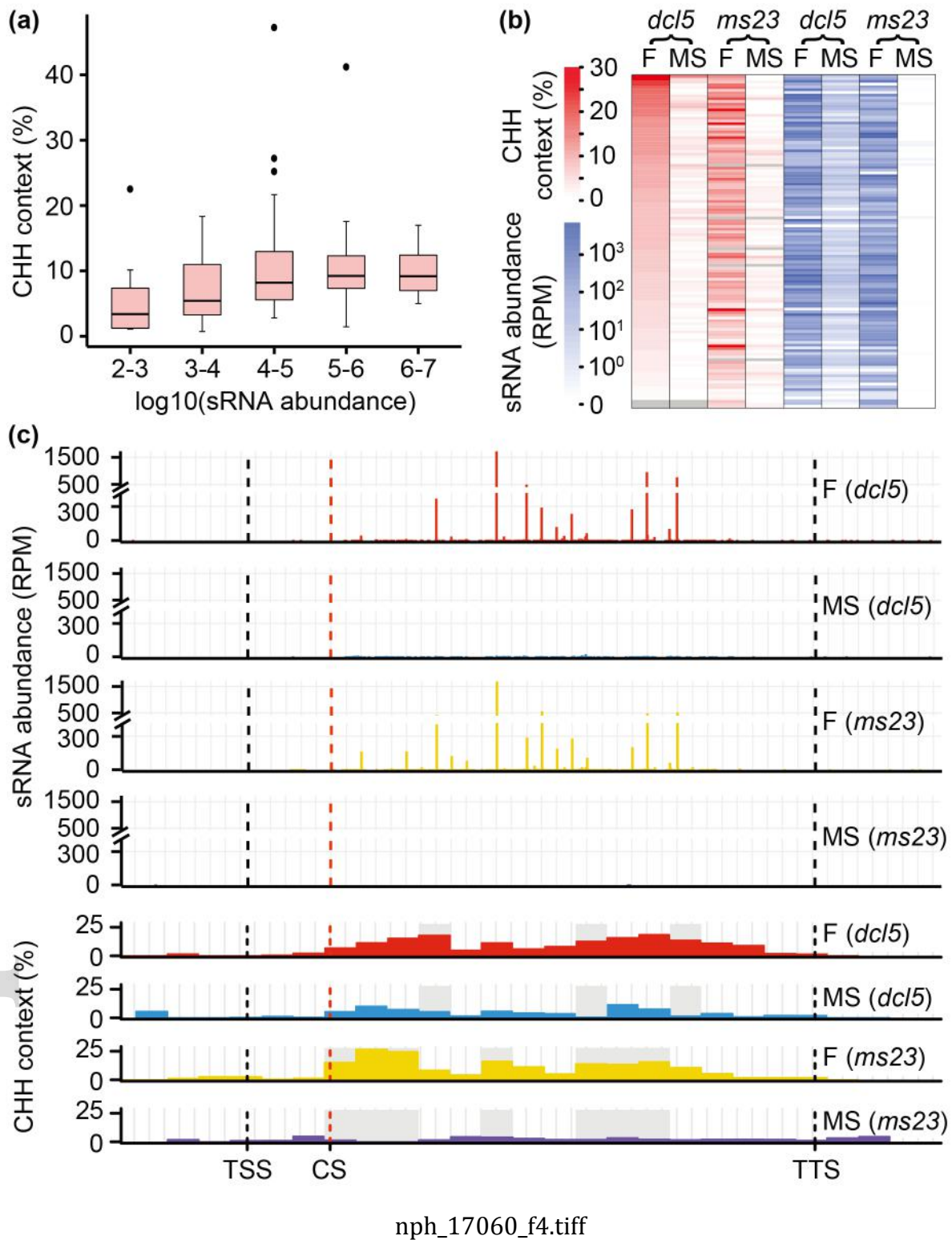


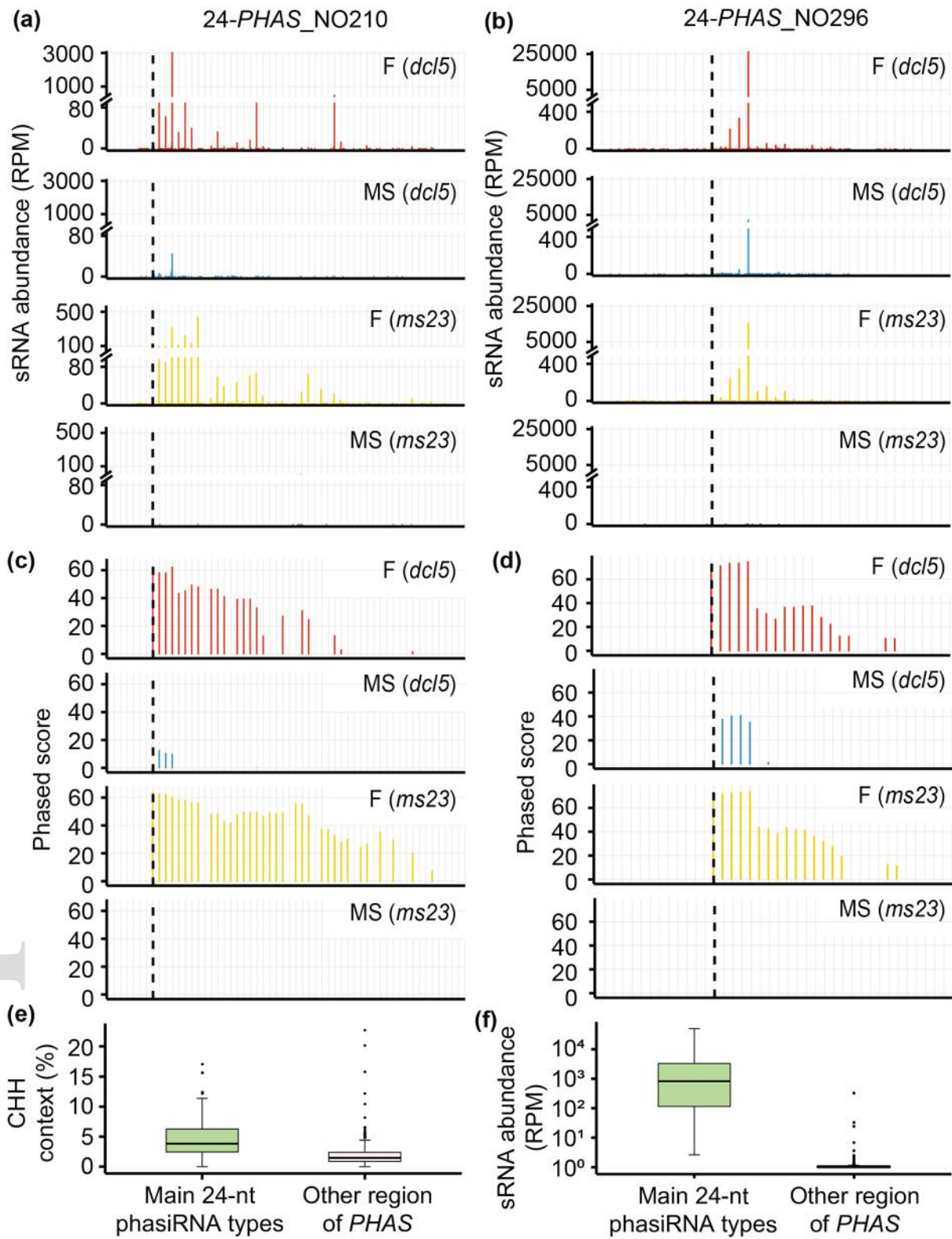
nph_17060_f1.tiff



nph_17060_f2.tiff







nph_17060_f5.tiff